Journal of Structural Geology 32 (2010) 350–361

Contents lists available at ScienceDirect

Journal of Structural Geology

journal homepage: www.elsevier.com/locate/jsg

Paleoseismic evidence from trench investigation along Hajipur fault, Himalayan Frontal Thrust, NW Himalaya: Implications of the faulting pattern on landscape evolution and seismic hazard

Javed N. Malik [a,*], Ajit K. Sahoo [a,1], Afroz A. Shah [a,2], Dattatraya P. Shinde [b], Navin Juyal [b], Ashok K. Singhvi [b]

[a] Department of Civil Engineering, Indian Institute of Technology Kanpur, Kanpur, UP, India
[b] Physical Research Laboratory, Ahmedabad 380 009, Gujarat, India

ARTICLE INFO

Article history:
Received 8 February 2009
Received in revised form
31 December 2009
Accepted 6 January 2010
Available online 14 January 2010

Keywords:
Active faults
Lateral propagation
Himalayan Frontal Thrust
Paleoseismology
Landscape change
Seismic hazard

ABSTRACT

The study area falls within the mesoseismal zone of 1905 Kangra earthquake (Mw 7.8). Two parallel NNW–SSE striking active fault scarps named as *Hajipur Faults* (HF1 and HF2) along the northwestern end of the Janauri anticline in the foothill zone, have displaced floodplain sediments of the Beas River. The HF1 and HF2 represent the imbricate faults of the Himalayan Frontal Thrust (HFT), and are the result of lateral propagation of deformation from two fold segments i.e., JF1 and JF2 respectively in northwest direction along the strike. Ground Penetrating Radar (GPR) profiles and trenching across the HF2 reveal two low-angle thrust fault strands (F1 and F2). Displacements of ~7.5 m on F2 and ~1.5 m on the associated branching faults (f_a, f_b and f_c) were observed. Total four stratigraphic units: unit A (gravel) – with a lens of medium sand (unit A′) is the oldest; overlain by units B – medium to coarse sand; unit C – with fine to medium sand; and unit D – fine to medium sand with scattered gravel were observed in trench. Radiocarbon ages of the charcoal samples from unit B and unit D, optical ages of sediments from units A′, B and C, GPR data and trench log, suggest two major events along F1 and F2 strands. Event I along F1 occurred during 2600–800 yr BP and Event II along F2 around 400 yr BP and before 300 yr BP. Given the uncertainty in dates it is suggested that the latest event occurred during 1500–1600 AD. Considering the oldest unit (unit A) exposed in trench with vertical displacement of 7.5–8 m, age of 2600 ± 500 yr BP and net displacement of ~9 m during single event along low-angle fault ($\theta = 25°$), implies slip rate = 7.6 ± 1.7 mm/yr, uplift rate = 3.2 ± 0.6 mm/yr, shortening rate = 6.9 ± 1.4 mm/yr and recurrence interval = 1160 ± 250 yr for large-magnitude event with Mw >7.0. With the recurrence of 1100 yr, the penultimate event probably occurred at around 1400–1500 yr BP. Given the recent GPS based slip rate of 14 ± 1 mm/yr in Kangra reentrant (Baneerjee and Burgman, 2002), the present study suggests that about half of this slip is consumed along the HFT and that this fault is more active compared to those in the hinterland.

1. Introduction

The continued convergence between Indian and Eurasian plates has made the Himalayan arc a seismically active region that experienced moderate to large earthquakes. In last 100 years the Himalaya has experienced three major large-magnitude events during 1905 Kangra (Mw 7.8), 1934 Bihar (Mw 8.1) and 1950 Upper Assam (Mw 8.4) earthquakes (Seeber and Armbruster, 1981; Yeats et al., 1997; Ambraseys and Bilham, 2000; Ambraseys and Douglas, 2004) (Fig. 1a). The recent October 8, 2005 Muzaffarabad earthquake (Mw 7.6) occurred along an earlier identified active fault named *Balakot–Bagh fault* causing extensive damage in Pakistan as well as in Indian side (Nakata, et al., 1991; Kaneda et al., 2008). Seismic hazard evaluation in Himalaya is one of the most crucial problems. Historic records and instrumental data available so far is not so comprehensive and also little or no written records are available from much of the Himalayan belt, hence actual appraisal of hazard from this dataset is difficult (Iyengar and Sharma, 1999; Bilham et al., 2001). For proper seismic hazard estimation,

* Corresponding author. Tel.: +91 512 2597723; fax: +91 512 2597395.
E-mail addresses: javed@iitk.ac.in (J.N. Malik), sahooajitkumar@gmail.com (A.K. Sahoo), afroz.shah@jcu.edu.au (A.A. Shah), singhvi@prl.res.in (A.K. Singhvi).
[1] Present address: Reliance India Limited, Mumbai, India.
[2] Present address: School of Earth and Environmental Sciences, James Cook University, Townsville, Queensland 4811, Australia.

0191-8141/$ – see front matter © 2010 Elsevier Ltd. All rights reserved.
doi:10.1016/j.jsg.2010.01.005

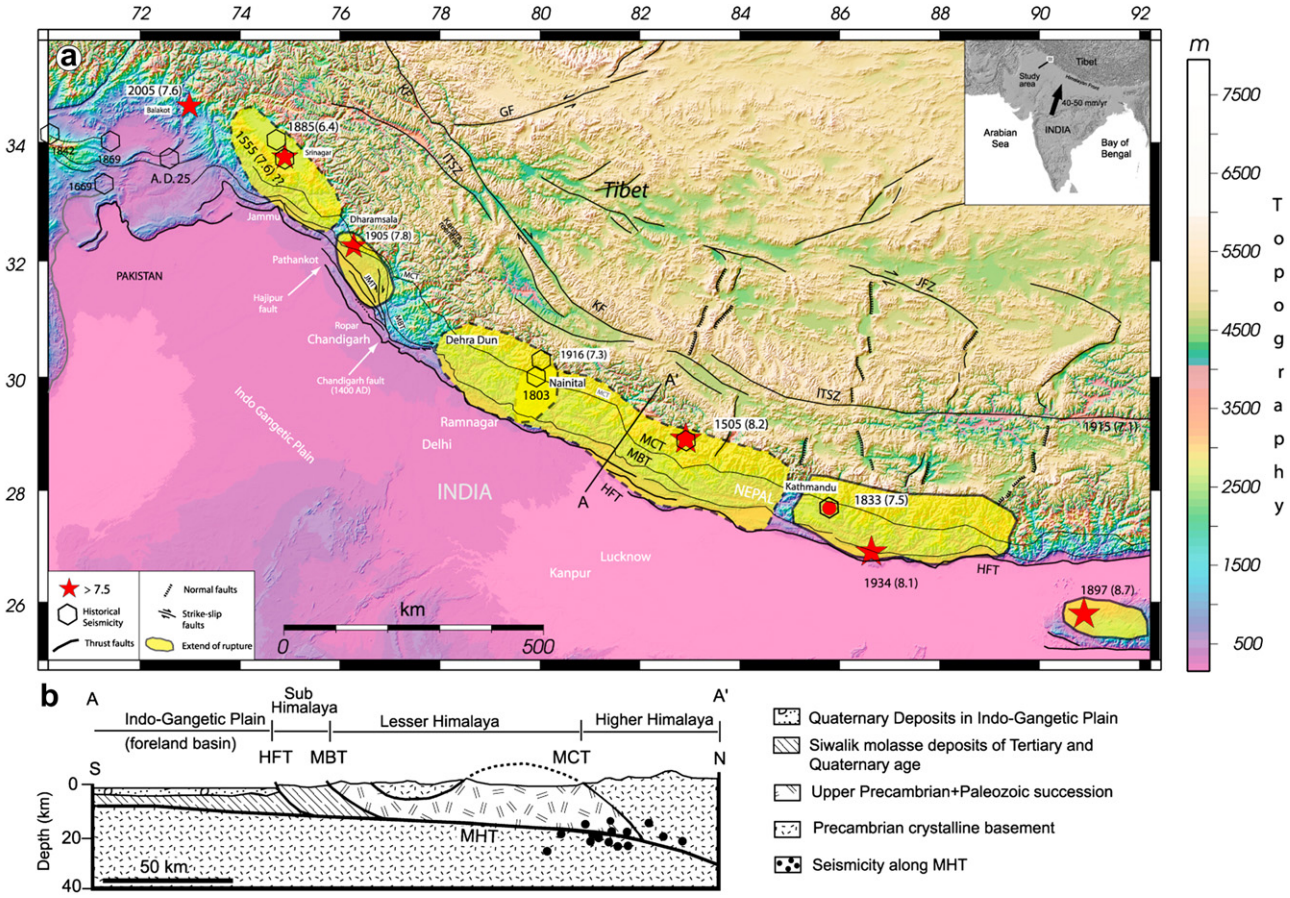

Fig. 1. (a) Map showing area of the Himalaya and its neighborhood with major fault systems, historic and recent large-magnitude earthquakes (after Nakata et al., 1990; Yeats et al., 1992; Powers et al., 1998; Wesnousky et al., 1999; Lavé and Avouac, 2000; Tapponnier et al., 2001; Kumar et al., 2001; Malik and Nakata, 2003). Extent of inferred rupture areas during 1505 (Mw 8.2), 1555 (Mw 7.6), 1905 (Mw 7.8), 1934 (Mw 8.4) are shown by shaded portion with dashed line (after Yeats et al., 1992; Ambraseys and Bilham, 2000; Ambraseys and Douglas, 2004; Bilham and Ambraseys, 2005). HFT – Himalayan Frontal Thrust, MBT – Main Boundary Thrust, MCT – Main Central Thrust, ITSZ – Indus-Tsangpo Suture Zone, JFZ – Jiali fault zone, KF – Karakoram fault, (b) North–South generalized geologic section across the Central Himalaya, seismicity along the Main Himalayan Thrust is marked by black dots (Ni and Barazangi, 1984). Location of the section is marked by A–A′ line in Fig. 1a (after Seeber and Armbruster, 1981).

identification of active faults bears significant importance, it is also necessary to know the accurate locations and geometry of active faults (Gross et al., 2002). Paleoseismic investigation is one of the most commonly adopted techniques towards identification/cataloguing the historic and pre-historic earthquakes in tectonically active regions of the world (McCalpin, 1996).

The studies carried out during several decades have provided important data on the ongoing crustal deformation in the Himalaya. However, not much effort is directed to site-specific studies (Nakata, 1989; Valdiya, 1992; Yeats et al., 1992; Wesnousky et al., 1999; Malik et al., 2003; Malik and Nakata, 2003). Recent paleoseismic investigations from India, Pakistan and Nepal along the Himalaya arc have added valuable information towards the occurrence of large-magnitude earthquake during recent historic past. Investigations along Sirmuri Tal fault in Dehra Dun valley along Main Boundary Thrust (MBT) suggests two major earthquakes have struck Dehra Dun region in the last 1000 years (Oatney et al., 2001). Paleoseismic investigations along Black Mango (Kala Amb) tear fault along the Himalayan Frontal Thrust (HFT) in the NW Himalaya have revealed evidence of two large earthquakes with surface ruptures during the past 650 years; subsequent to 1294 AD and 1423 AD and yet another at about 260 AD (Kumar et al., 2001). Also studies from NW Himalaya have indicated major event at around ~1400–1500 AD along HFT (Kumar et al., 2006; Malik et al., 2008). Paleoseismic evidence from east central Nepal reveals a single earthquake rupture along the Frontal Thrust during ~1100 AD (Lavé et al., 2005). Trench investigation performed along Balakot–Bagh fault after the 2005 Muzaffarabad earthquake suggests recurrence interval of 1000–3300 yr and shortening rate of 1.4–4.1 mm/yr (Kaneda et al., 2008).

Earthquakes along active faults are periodic (Yeats et al., 1997; McCalpin, 1996) and a proper seismic hazard assessment needs an active fault map with paleoseismic history. The Muzaffarabad 2005 event has raised more concerns towards the seismic hazard assessment in areas along Himalayan foothills, where practically no historic or no active fault-paleoseismic data is available. In this paper we document the geomorphic manifestation of newly identified active faults, named as *Hajipur faults* in the mesoseismal zone of 1905 Kangra earthquake (Mw 7.8) along the northwestern end of the Janauri anticline (Fig. 1a). These faults along the Himalayan front were identified using CORONA satellite (stereo pair) photos, Digital Elevation Model (DEM) generated from SRTM data followed by detail field investigations (Figs. 2–4). GPR (Ground Penetrating Radar) profiling was conducted to understand the geometry of the faulting and to locate the appropriate site for further paleoseismic investigation. Paleoseismic investigation revealed occurrence of two major events during 2600–800 yr. BP and another at around 400 yr BP. The 1905 Kangra and 2005 Muzaffarabad events are the only well documented events from NW Himalaya (Iyengar and Sharma, 1999; Ambraseys and Jackson,

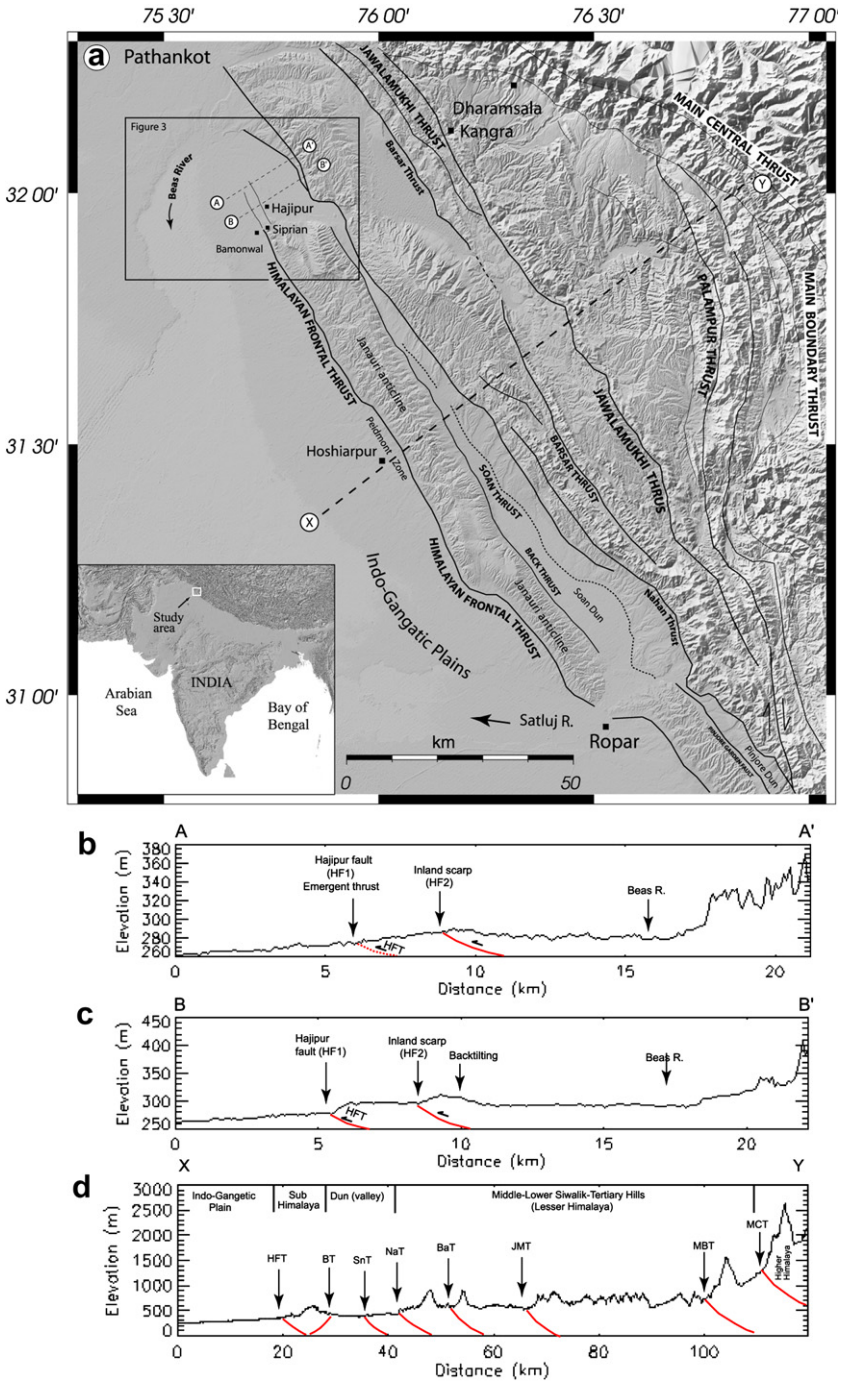

Fig. 2. (a) Shaded relief map showing distribution of major faults and geomorphic divisions of the NW Himalaya (modified after Malik and Mohanty, 2006). Box on top left marks area of Fig. 3. Three topographic profiles extracted from SRTM data are marked by dotted line, these lines are A–A′ and B–B′ across the northern fringe of Janauri anticline, and X–X′ across the central portion of Janauri anticline extending in NE–SW covering the Indo-Gangetic Plain in the south up to Higher Himalaya in north, (b) Topographic profile across the Hajipur fault – HF1 and HF2 along the northern fringe of Janauri anticline. The profile A–A′ shows very low scarp along HF1 and HF2, scarps are marked by arrows. The scarp along HF1 is marked by gentle sloping surface, where slight elevation change is seen along HF2. The deformation is a result of movement along the northeast dipping thrust faults (HF1 and HF2), (c) This profile extracted close to the hill range towards southeast shows about 10 m and 8 m high scarp along HF1 and HF2 respectively. Slight back-tilting of uplifted surface towards NE is clearly noticed along HF2, and (d) This profile shows relative topographic variations between Indo-Gangetic Plain in the south and Higher Himalayas in the north. The sharp topographic breaks are indicative of north dipping thrust faults, except in the frontal portion with a south dipping back-thrust.

2003; Malik et al., 2007; Kaneda et al., 2008). And also up to now, surface ruptures associated with the 2005 event (Yeats and Hussain, 2006; Kaneda et al., 2008) and historic events during 1100 AD and 1400–1500 AD are the only coseismic features known so far along the Himalaya thrust (Lavé et al., 2005; Kumar et al., 2006; Malik et al., 2008). It has been suggested that the 1905 earthquake rupture corresponds to the Jawalamukhi Thrust (JMT, Fig. 1a) and that the slip was never transferred to the HFT (Wallace et al., 2005), this is consistent with our trench results. Moreover, the historical records of pre-1905, major earthquake in Kangra are not available (Bilham, 2001). The historical catalogue from this area and further northwest reports the occurrence of two earthquakes in 1555 AD

Fig. 3. (a) Mosaic of CORONA satellite photo showing distribution of newly identified active fault traces named as "Hajipur faults" – HF1 and HF2 on the left bank of Beas River near Hajipur village. Boxes show location of trenches and GPR profile line across the HF2 fault scarp. Empty arrow marks the direction of fault propagation towards NW. The length of HF2 fault is more compare to the frontal HF1 fault. The greater lateral extend of HF2 fault in terms of length suggests young tectonic movement along this fault. Uplift of floodplain deposits along HF1 and HF2 has been responsible for the shifting/deflection of the Beas River channel along it present course. The present "U-shaped" turn of Beas channel is a result of lateral propagation of faults. Tectonic deformation has been propagated to HF1 and HF2 from JF1 and JF2 (fault-related-folds) respectively, and (b) Panoramic view of HF2 – Hajipur fault scarp towards hinterland side. Scarp height is about 8 m. Arrows marks location of trench sites – T1 and T2.

(Mw 7.6) and in 1885 AD (Mw 6.4) in the Kashmir valley. It is quite possible that the latest event in our trench represents the event occurred during 1500–1600 AD. The information generated by us will be of great importance since no paleoseismic information is available from this region of NW Himalaya.

2. General seismotectonic background

Since the collision (~50 Ma) along the Indus-Tsangpo Suture Zone (ITSZ), successive deformation zones have progressively advanced southward towards foreland, causing faulting and folding along the south verging prominent structural features [Gansser, 1964; Seeber and Armbruster, 1981; Lyon-Caen and Molnar, 1983]. These principal intracrustal thrusts are the Main Central Thrust (MCT), the Main Boundary Thrust (MBT), and the Himalayan Frontal Thrust (HFT) (Fig. 1a and b). These thrusts with an average dip of about 30°–40° northwards mark distinct geological boundaries, to the north the boundary between the Lesser Himalayan sedimentary and metasedimentary rocks is marked by the MBT, and between Lesser Himalayan and the Higher Himalayan Crystallines, by the MCT (Valdiya, 1980). The HFT, displacing the Siwalik (Powers et al., 1998) demarcates the boundary between the foreland fold (Siwalik range) composed of late Tertiary to early Quaternary molassic sediments (Upper Siwalik) and the undeformed Quaternary alluvial deposits of Indo-Gangetic Plain (Raiverman et al., 1994; Powers et al., 1998). Occurrence of 5–50 m high discontinuous fault scarps displacing the Late Quaternary and Holocene alluvial-fan surfaces and fluvial terraces along the MBT and HFT suggests recent tectonic movements (Nakata, 1972, 1989; Yeats et al., 1992; Valdiya, 1992; Wesnousky et al., 1999; Kumar et al., 2001; Malik and Nakata, 2003; Malik et al., 2003). It is suggested that these major thrusts converge towards north and merge into a décollement, the Main Himalayan Thrust (MHT) (Seeber and Armbruster, 1981; Zhao et al., 1993; Brown et al., 1996; Hodges, 2000; Hodges et al., 2004) (Fig. 1a and b).

Tectonic models proposed for the evolution of Himalaya suggest that the zone of plate convergence gradually moved towards foreland (e.g. Powell and Conaghan, 1973; LeFort, 1975; Stöcklin, 1980). It is also suggested that at each stage, the deformation was taken up by a newly formed younger tectonic structure and older fault systems became inactive. This means MBT is active and MCT is dormant. Later the deformation moved on to the front along HFT which marks

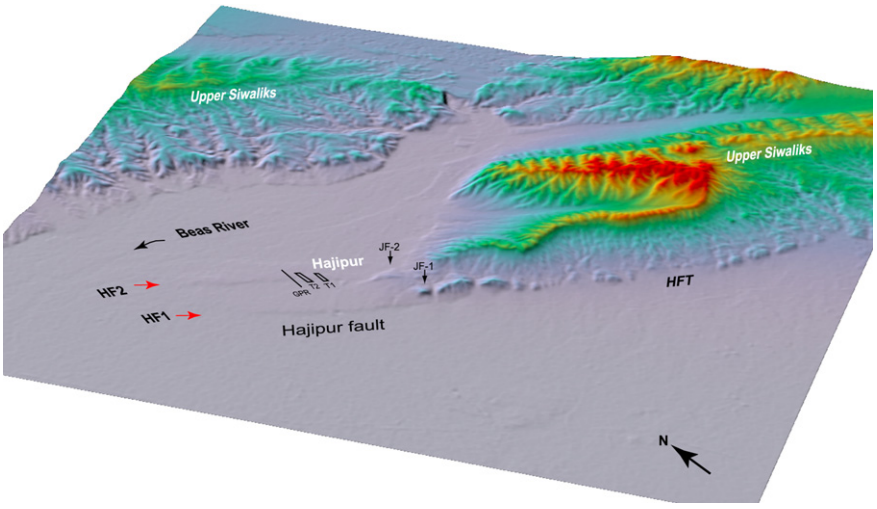

Fig. 4. DEM (3D) of the area around the north fringe of the Janauri anticline (the frontal foreland fold) in the foothill zone of NW Himalaya. Two traces of faults named as "Hajipur fault" – HF1 and HF2 have displaced the young Quaternary sediment succession which belongs to the older floodplain of Beas River resulting into formation of SW facing fault scarps. The fault scarps/traces are marked by red arrows, HF1 marks the frontal fault and HF2 is the hinterland fault. The height of the fault scarps reduces and die-outs towards NW, suggestive of lateral propagation of faulting-folding towards NW. Two boxes on the HF2 are the location of trench sites. The HF2 shows greater extending as compare to HF1, suggests recent movement and comparatively more active than HF2. The uplift of the floodplain along the HF1 and HF2 – branching of Hajipur faults caused deflection of Beas River along its present course. JF1 and JF2 represent fault-related-folds. (For interpretation of the references to colour in this figure legend, the reader is referred to the web version of this article.)

the southernmost limit of the Himalayan orogenic belt (Validya, 2003). The steady-state model proposed, also suggested a gradual shift of the deformation towards the foreland, with MBT and MCT as contemporaneous features and MCT is still active (Seeber et al., 1981; Seeber and Armbruster, 1981). This is supported by knick points observed in river profiles which cross the MCT and from the evidence of uplifted terraces in the Higher Himalaya (Seeber and Gornitz, 1983). Moreover, several geological and geomorphological evidences indicate ongoing tectonic activity along the MCT (Valdiya, 1980; Seeber and Gornitz, 1983) as well as along the MBT (Valdiya, 1992; Nakata, 1989; Malik and Nakata, 2003).

Within the last decade, several studies focusing on convergence rates have provided an opportunity to compare the short-term shortening rates measured by GPS with the long-term rates estimated from geological and geomorphological studies. Based on the NUVEL-1A model (DeMets et al., 1994), India moves northward with respect to Asia at a rate of ≈40 mm/yr in the west to ≈52 mm/yr in the east (Bilham and Gaur, 2000). GPS measurements determined that the India–Eurasia plate convergence rate increase from 37 to 44 mm/yr, from west to east along the Himalayan arc (Banerjee and Bürgmann, 2002). On the basis of the geological, geomorphological and GPS studies it has been suggested that 50% of the total convergence is consumed along the Himalayan arc, and the remainder of about 30% is taken up by the continental deformation further north within the Eurasian plate (England and Molnar, 1997; Avouac and Tapponnier, 1993; Wesnousky et al., 1999; Lavé and Avouac, 2000; Bilham et al., 2001; Kumar et al., 2001; Oatney et al., 2001; Banerjee and Bürgmann, 2002; Malik and Nakata, 2003). While the total convergence rate between India and stable Eurasia seems not well determined (see Bilham and Gaur, 2000 for difference between NUVEL-1A and GPS), whereas, the short-term geodetic rates and the long-term geological rates seem to be consistent along the Himalayan front.

GPS measurements in Nepal suggest that India and southern Tibet converge at a rate of about 20 ± 3 mm/yr (Bilham et al., 2001). This short-term rate is consistent with the long-term rate of 21 ± 1.5 mm/yr deduced from dating of folded terraces across the Siwalik Hills in central Nepal Himalaya (Lavé and Avouac, 2000). Recent GPS measurements carried along western Himalaya determined a lower rate of 14 ± 1 mm/yr (Banerjee and Bürgmann, 2002). This rate is consistent with the shortening rates deduced from the restoration of balanced geological cross-section across the fold and thrust belt in the Himalayan frontal portion between the HFT and the MBT, with a rate of 14 ± 2 mm/yr across the Kangra reentrant and 11 ± 5 mm/yr across the Dehra Dun reentrant (Powers et al., 1998). Rates determined from geomorphological and paleoseismic investigations suggest a slip rate of 13.8 ± 3.16 mm/yr near Mohand in the Dehra Dun region (Wesnousky et al., 1999), 9.62 + 7.0/−3.5 mm/yr along the Black Mango tear fault (Kumar et al., 2001), and about 6.3 ± 2 mm/yr near Chandigarh (Malik and Nakata, 2003) are also consistent with the above rates.

3. General geomorphological setting

In this study we use high resolution CORONA KH-4B satellite data (stereo pair, ground resolution ~6 feet) of September 1971, Shuttle Radar Topographic Mission (SRTM) 3 arc second data (resolution ~90 m) and Survey of India (SOI) topographic maps (scale 1: 50,000) in order to map active faults and landforms. Field investigations allow us to identify two active fault traces on the left bank of the Beas River (Figs. 1a, 2a, 3a and 4).

The Himalayan belt in northwestern portion of the arc is widely distributed in 100 km wide N–S zone (Fig. 2a and d). Geomorphologically the area can be broadly classified into four zones, from north to south (Nakata, 1972; Powers et al., 1998; Malik and Mohanty, 2007). These zones are bounded to south by major thrust faults, (1) folded mountain range of Higher Himalaya (>3000 m) comprised of Mesozoic and older metasedimentary rocks are separated from Lesser Himalaya hills (~2000 m) made up of late Proterozoic–early Cambrian rocks by Main Central Thrust (MCT) in the south. Along with this the area further south between the Main Boundary Thrust (MBT) and Soan Thrust (SnT) is marked by several NNW–SSE trending fold ranges bounded to their south by major thrust faults, viz. Palampur Thrust (PaT), Jawalamukhi Thrust (JMT), Barsar Thrust (BaT) etc. These hills consist of inter-layered succession of conglomerate, sandstone, claystone etc., of Lower and Middle Tertiary sediments. (2) In the frontal part another prominent geomorphic feature is marked by a longitudinal intermontane

valley locally know as *Soan Dun*. This valley is filled by thick alluvium of late Pleistocene to Holocene age overlying the Middle and Lower Siwalik succession represents the debris deposited by coalesced alluvial-fan and finer fluvial deposits. Soan Dun is bounded to its north by Lower Tertiary hills known as Bharwani anticline (350–650 m) in northwestern part of the arc and to the south by Upper Siwalik (Sub-Himalaya) hills – the Janauri anticline. The Nahan Thrust (NaT) marks the boundary between the Lower Tertiary hill and Soan Dun. (3) The NNW–SSE striking Janauri Anticline (400–650 m) composed of Mid-Miocene to late Pleistocene age molassic sediments (Upper Siwaliks) marks the Sub-Himalaya range which represent the southernmost fringe of the Himalaya. This range is separated from the Indo-Gangetic Plain in the south by Himalayan Frontal Thrust (HFT). The frontal fold along it back limb is bounded by south dipping back-thrust (Powers et al., 1998). (4) The vast Indo-Gangetic Plain which represents the present foreland basin comprised of young Quaternary fluvial and alluvial-fan sediment succession deposited by the drainage debauching on the plain. The Janauri anticline does not seem to be extending further northwestward (Figs. 2a, 3b and 4), however, the extension is seen taken over by two younger faults (Figs. 2b, c, 3a and 4). The overall drainage network suggests that the Beas River is one of the major Himalayan river debauch on the alluvial plain, is marked by comparatively wider channel ranging from 5 to 8 km wide with prominent U-shape meander (Figs. 2–4).

3.1. Active fault distribution

Interpretation of CORONA KH-4B satellite photos and SRTM data helped in identifying the fault scarps. In this paper, the active faults are defined as one those ruptured repeatedly during the Late Quaternary, and are capable to generate rupture on the surface in future. The manifestation of young deformation along the fault is always reflected on the surface in form of the deformed geomorphic feature such as active fault scarps or warped surface. Based on prominent elevation change trace of two linear features – the *Hajipur fault* (HF1 and HF2) extending for about 8–10 km with NNW–SSE strike along the northwestern end of the Janauri anticline were identified on CORONA satellite photos and with the help of DEM extracted from SRTM data (Figs. 2–4). The HF1 – fault scarp along the front and HF2 in the hinterland side on the left bank of Beas River, have displaced/uplifted the floodplain deposits of the Beas River, resulting into formation of WSW facing scarps. The scarp height along HF1 and HF2 varies along the strike, marked with higher elevation near the range front and gradual reduction in NNW direction (Figs. 2a–c and 4). The height varies from 2 to 15 m. HF1 and HF2 are ~2.5 km apart and tectonic movements along these faults produced a stepped topography (Fig. 2a–c). Near the range front along HF2, distinct gentle back-tilting of about 6°–8° towards NNE direction was observed. Along the strike HF1 extends laterally for 8–8.5 km, and HF2 for 10–10.5 km (Figs. 2a–c and 4). The scarp height is 10–12 m along the HF1 near Bamonwal-Siprian villages, and reduces up to 8 m and as low as 2 m along the strike in NNW direction (Figs. 2a–c, 3a and 4). The scarp height along HF2 ranges from 6 to 8 m near the range front and reduces up to about 1.5 m along the strike (Figs. 2b, c and 4). Finally, both the scarps die-out towards near the tip (Fig. 4). The surface morphology of the scarp along HF1 is highly diffused and degraded compared to HF2 (Figs. 2–4). The sharp geomorphic contact and less degraded scarp along HF2 are indicative of younger displacement during recent geological past. Also the greater lateral extend of HF2 fault in terms of length justifies that younger movement has occurred along this fault (Fig. 4).

It has been suggested that any displacement related to normal or reverse faulting or on elastic crack will propagate laterally as well as vertically and marks reduction towards the ends along the strike (e.g., Gudmundsson, 1987a,b, 2000; Cartwright et al., 1995; Walsh et al., 2002; Davis et al., 2005). The decrease in displacement at the lateral ends (tips) of the faults or cracks will lead towards reduction of surface manifestation of deformation on ground (Gudmundsson, 1987a,b, 2000). The same was observed along the HF1 and HF2 scarps. The higher elevation of the scarp near the hill range as compared to the tip area indicates large displacements. A north-westward gradual decrease in heights of HF1 and HF2 scarps suggests lateral propagation along the strike and growth of associated folds (Figs. 2–4). Assuming that the folds grow by successive coseismic movements along the fault, it can be suggested that overall slip was accumulated during more than one major event (Walsh et al., 2002). Such lateral propagation of folds has resulted in diversion of rivers in active thrust-and-fold belt (Delcaillau et al., 1998; Champel et al., 2002; Bés de Berc et al., 2005; Malik and Mohanty, 2007). Thus, the deflection–diversion of the Beas River is attributed to northward propagation of faults (Figs. 3a and 4). According to Burbank et al. (1992) occurrence of parallel multiple fault lines are suggestive of imbricated fault system, commonly observed in thrust-and-fold belts. The surface distribution of two parallel faults HF1 and HF2 suggests the existence of an imbricated fault system and propagation of the tectonic activity from two fault-related-fold segments – JF1 and JF2 respectively (Figs. 3a and 4). Based on morphological characteristic and length of both the faults suggest that hinterland HF2 fault is more active as compared to HF1, and has accommodated most recent movements.

4. Georadar survey and paleoseismic investigation

With an aim to identify most recent events in the area, the Ground Penetrating Radar (GPR) survey was carried out across the HF2 fault scarp. GPR survey using a 200 MHz shielded antenna with SIR 3000 system (Geophysical Survey System Inc.) was carried out to confirm shallow subsurface faulting and to locate appropriate trenching sites along HF2 (Figs. 3 and 5a). Several profiles helped optimize acquisition parameters (Table 1), and finally a 32 m long profile with 7–8 m penetration depth was collected. High signals to noise ratio implied direct use of data without signal processing. Topographic corrections and auto gain control (AGC) enhanced the display resolution. Stacking was applied to avoid stretching of the data due to topographic correction.

Based on the prominent offsets and warping observed in the georadar reflections two low-angle thrust faults strands F1 and F2 were identified (Fig. 5a and b). Strands F1 identified between 19 and 28 m horizontal distance and F2 between 8 and 26 m marker are shown in Fig. 5b. Warping of radar reflections on the hanging wall of F1 fault at 18–22 m markers was seen; also similar deformed reflectors were noticed below the fault plane of F2 strand between 14 and 20 m markers on the footwall side. The F1 merges with F2 between 18 and 19 markers at a depth of about 5 m. F2 further continues towards the surface, traceable up to 8 m marker (Fig. 5b). The offset could be observed up to the surface with a deformation near the tip along F2.

We excavated two trenches (T1 and T2) across the HF2 fault scarp (Figs. 3b, 4, 6 and 7). Trench – T1 is about 7 m long, 1–2 m deep, and ~2m wide. Four stratigraphic units from A (older) to D (younger) were identified (Fig. 6). The exposed trench section revealed a very low-angle fault displacing units A and B over unit B. Internal folding is well noticed by the preferred orientation of the gravel clasts. Trench – T2 (18 m long, 1–4.5 m deep and 2–2.5 m wide) revealed excellent deformational features. In this paper we discuss trench – T2 in greater detail (Fig. 7a and b). Similar to T1, four stratigraphic units were identified in T2. Unit A, about 1.5–3.0 m thick is made of rounded to sub-rounded poorly sorted

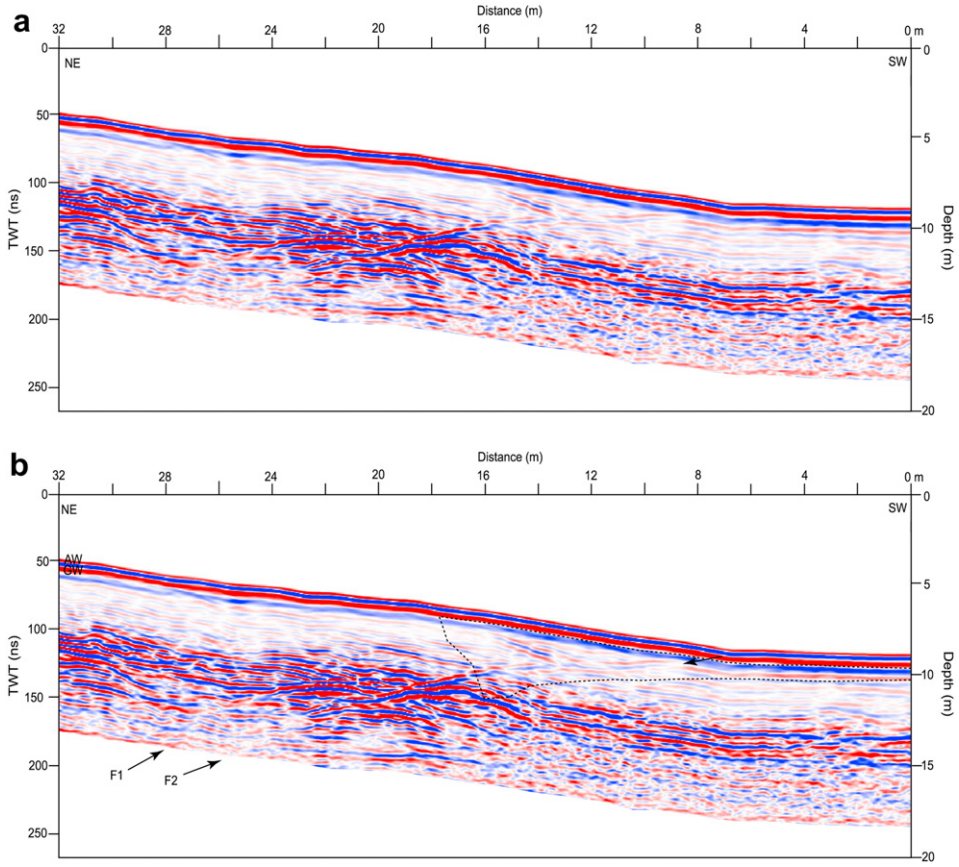

Fig. 5. (a) Unprocessed 32 m long Ground Penetrating Radar (GPR) profile collected with 200 MHz antenna across Hajipur fault (HF2), (b) Processed profile showing two low-angle thrust fault strands F1 between 19 and 28 m, and F2 between 8 and 26 m horizontal distance marker. Warping of radar reflections was identified on the hanging wall of F1 fault at 18–22 m markers, and on the footwall side below the fault plane of F2 strand between 14 and 20 m markers. F1 merges with F2 between 18 and 19 markers. F2 continues near to the surface up to 8 m marker showing prominent deformation. The data is shown in the form of line-scan, which represents the amplitudes, Red is positive pulse and Blue marks negative pulse. TWT-two way travel time in nanosecond (ns). The box with dotted line shows approximate trench area. AW – Air wave and GW – Ground wave. The dotted line shows the location of trench area across the scarp. (For interpretation of the references to colour in this figure legend, the reader is referred to the web version of this article.)

cobble-pebble, weakly stratified fining upwards sequences, with occasional occurrence of lens shaped medium sand (unit A′). This unit shows channel deposit. Unit A was overlain by about 2.5 m thick massive medium to coarse sand unit – Unit B. The lower part unit B (1.5 m) comprises more clayey silt package with blocky structures compared to the upper part, whereas the upper 1 m part shows occasional laminations and scattered pottery fragments. Looking to the proximity of the Beas River it is suggested that, unit B represents its older floodplain, deposited under overbank environment during flooding condition. Unit C (0.5 m) comprising medium to coarse sand got deposited during the phase of scarp degradation (Fig. 7b). Unit D, about 0.2–0.4 m thick capped the overall succession, comprised medium to fine sand with dispersed gravels having shallow channel-trough geometry, which can be interpreted as a channel-fill.

Table 1
Acquisition parameters for GPR survey across Hajipur fault (HF2-hinterland), NW Himalaya foothill zone.

Acquisition	Parameters GPR survey
Antenna	200 MHz
Sample/scan	512
Bits/sample	16
Rate (scans/s)	60
Scans/m	50
IIR (Infinite Impulse Response) filter	Low pass 300 MHz High pass 20 MHz
Dielectric constant	4

Only F2 dipping towards NE was observed in the trench (Fig. 7). The dip of F2 was ~32° at a depth in the northeast of trench and graded to ~8° to almost horizontal in the southwest near surface. The F2 splayed into three branching faults: f_a, f_b and f_c near the surface. The faulting along F2 strand as well as branching faults displaces the unit A (gravel) and unit B (massive sand) indicative of one single event. These units (A and B) show prominent folding along low-angle fault. We surmise that the faulting along all these faults is coeval since they all are covered by unit C. The flattening of fault geometry has been observed in the trenches excavated across the El-Asnam fault in Algeria (Meghraoui et al., 1988), in the Himalaya across Chandigarh fault (Malik et al., 2003, 2008) and in Pakistan across the fault scarp related to 2005 Muzaffarabad earthquake (Kaneda et al., 2008; Kondo et al., 2005).

The displacement measured along the F2 strand taking into consideration the bounding surface between the units A and B exposed in the trench suggests that these units have been displaced by about ≥7.5 m during recent event (Fig. 7b). The folding of these units along the fault suggests that part of the slip has also been consumed in folding. In addition to this the branching faults (f_a, f_b and f_c) show displacement of ≥0.4 m, ≥0.5 m and ≥0.5 m respectively. Therefore, adding the displacement along the main (F2) as well as the splayed faults gives a total slip of ~8.5–9 m during single event.

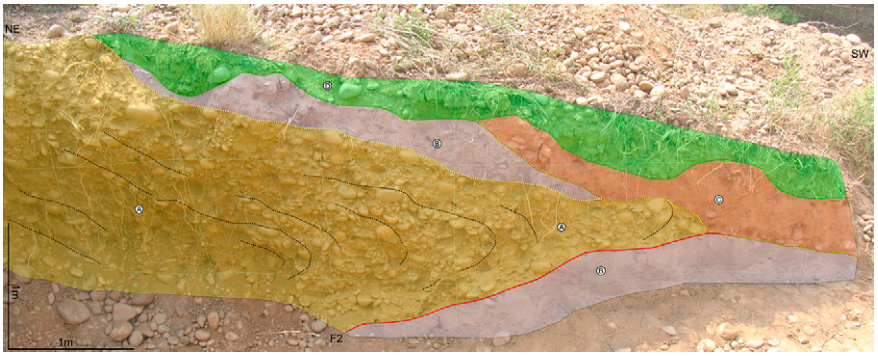

Fig. 6. North wall of 7 m long and 1–2 m deep trench T1 excavated across Hajipur fault (HF2). The exposed trench section shows four major lithounits, unit A – gravel, unit B – massive sand, unit C – medium to fine sand capping the faulted units, and unit D – topmost unit capping the overall sequence. A low-angle thrust fault has displaced units A and B. The clast fabric in unit A reveals folding. For location refer Figs. 3 and 4.

Based on the GPR profile and exposed trench section it is suggested that at least two major events have been experienced along this HF2. The event sequences of faulting can be constructed as, Stage I – Event I, faulting along F1, displacement of unit A (Fig. 8a); Stage II – deposition of unit B (Fig. 8b). The blocky nature of the lower part of unit B compared to the upper part, suggests that probably there was break in deposition. Later during next phase of deposition the upper part of unit B was deposited under same overbank environment (Fig. 8b). Stage III – Event II, displacement of units A and B by $\geq$7.5 m along F2 and along f_a, f_b and f_c with total slip of ~9 m (Fig. 8c). Movement occurred after the deposition of unit B. Stage IV – erosion, deposition of units C and D (Fig. 8d).

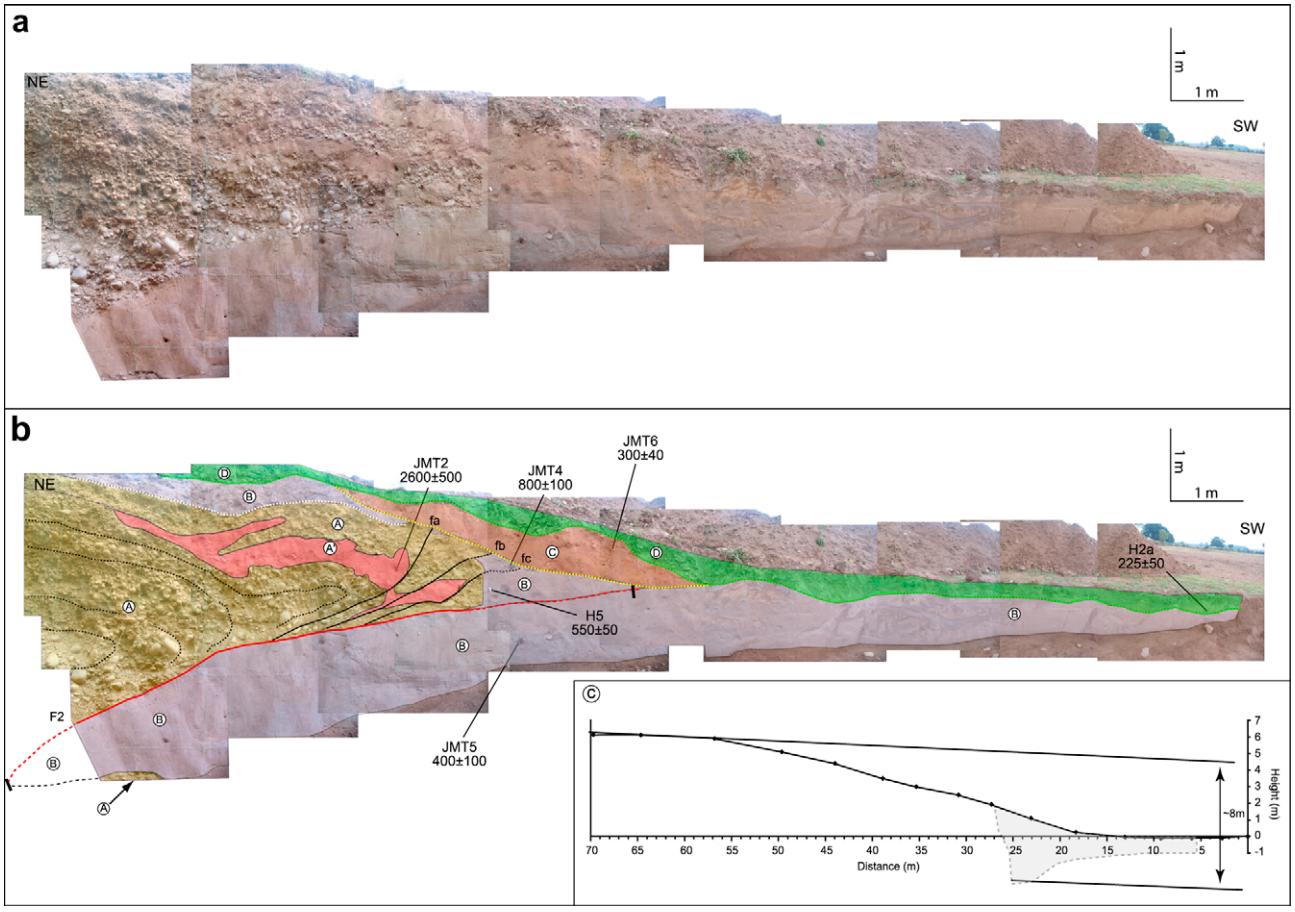

Fig. 7. (a) North facing wall of 18 m long trench section excavated across Hajipur fault (HF2), (b) The trench wall revealed only F2 strand. The exposed successions show four major lithounits. Unit A – gravel deposits and A′ is sandy unit embedded within the grave unit, Unit B – massive sand unit, Unit C comprising medium to coarse sand, and Unit D comprised of medium to fine sand capping the sequence. Both units A–A′ and B have been displaced along the F2 strand. The NE dipping F2 strand is marked with variable dip of ~32° in deeper part of the trench and to ~8° to almost horizontal in the southwest near surface. Total displacement of about 8–9 m (i.e. ~7.5 m along the main fault and 1.5 m along the branching faults (f_a, f_b and f_c)) was measured in trench. Location of samples dated by OSL and AMS are marked on the trench, (c) Topographic profile collected with total station shows scarp height of about 6 m. The oldest unit A shows total vertical displacement of about 8 m measured between the top of the exposed gravel in the trench and top on the scarp in the hanging wall. For location refer Figs. 3 and 4.

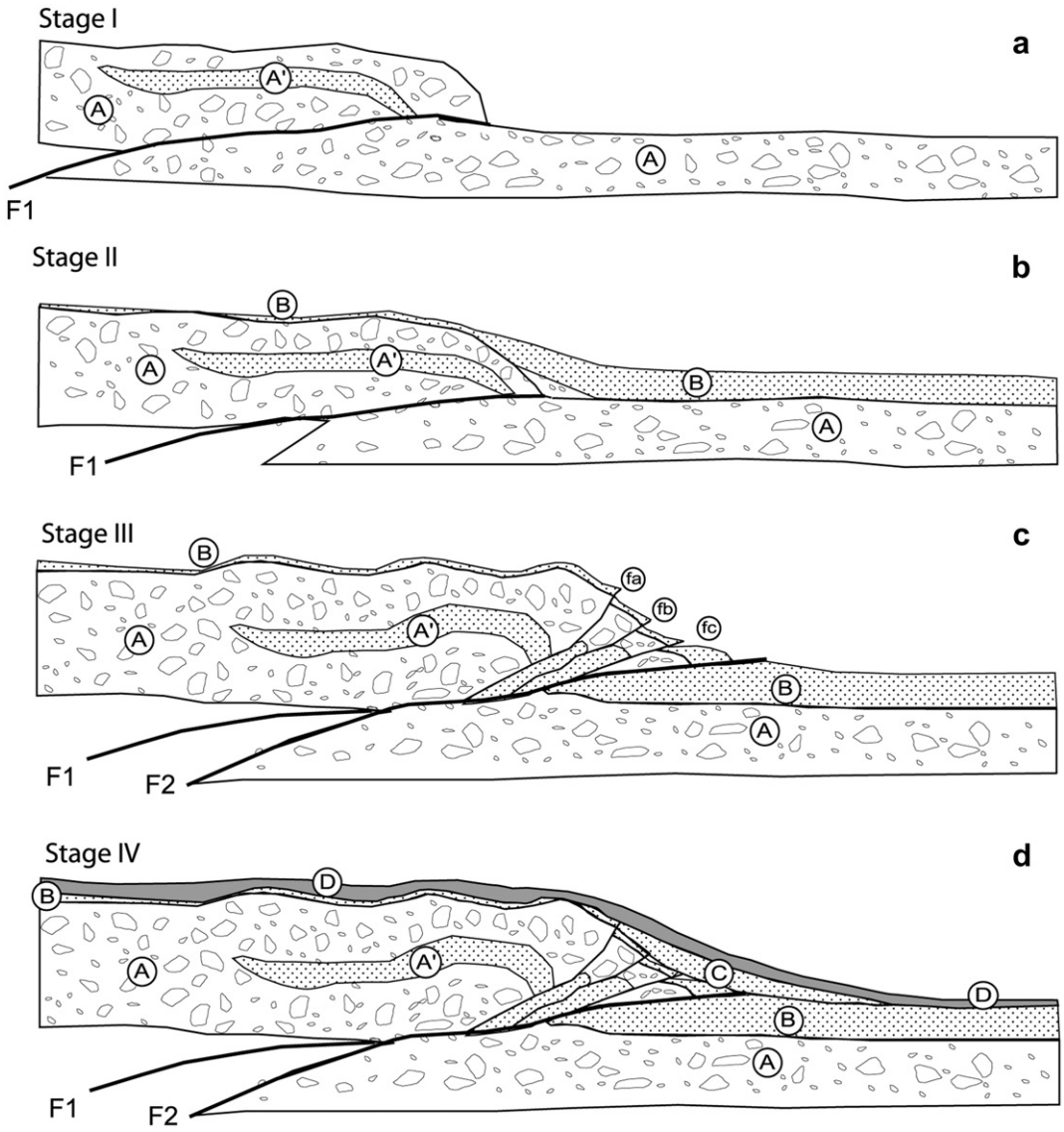

Fig. 8. Schematic view of trench log showing sequence of faulting and depositional phases from Stage I to IV. (a) Stage I: Displacement of unit A–A′ along F1 strand marking Event I, (b) Deposition of unit B, (c) Event II: displacement of unit A–A′ and unit B along new branching out fault strand F2, and (d) deposition of unit C and finally capping by unit D.

5. Chronology of events

Optically Simulated Luminescence (OSL) of sediments and radiocarbon Accelerator Mass Spectroscopy (AMS) of detrital charcoal were used for the chronology of stratigraphy and related faulting events (Tables 2 and 3). OSL dated the depositional event of the sediment and radiocarbon ages dated charcoal associated with the sediment. OSL ages are calendar ages whereas radiocarbon ages

Table 2
Radiocarbon ages.

Location of the sample[f]	Sample number	Lab sample number[a]	$\delta^{13}C(‰)$[e]	Conventional age[b]	Corrected pMC[d]	Radiocarbon age (BP)	Calibrated age 2σ[c]
Unit D	H2a	KIA30702	-27.84 ± 0.13	225 ± 50 BP	97.22 ± 0.59	226 ± 49	cal A.D. 1623–1696 (probability 30.8%) A.D. 1725–1814 (probability 37.6%)
Unit B	H5	KIA30705	-27.78 ± 0.19	550 ± 50 BP	93.39 ± 0.57	549 ± 49	cal A.D. 1302–1370 (probability 44.8%) A.D. 1381–1440 (probability 50.6%)

[a] Samples were processed and measurements were carried out at Leibniz Labor für Altersbestimmung und Isotopenforschung Christian-Albrechts-Universität Kiel.
[b] Conventional ^{14}C ages were calculated according to Stuiver and Polach (1977) with a $\delta^{13}C$ correction for isotopic fractionation based on the $^{13}C/^{12}C$ ratio measured by our AMS-system simultaneously with the $^{14}C/^{12}C$ ratio.
[c] "Calibrated" or calendar ages were calculated using "CALIB rev 4.3" (Dataset 2, 1998 decadal atmospheric data), Stuiver et al. (1998).
[d] "Corrected pMC" indicates the percent of modern (1950) carbon corrected for fractionation using the ^{13}C measurement.
[e] Please note that the $\delta^{13}C$ includes the fractionation occurring in the sample preparation as well as in the AMS measurement and therefore cannot be compared to a mass spectrometer measurement.
[f] Refer trench section Fig. 7b for sample location.

Table 3
OSL dating.

Location of the sample[a]	Sample number	Th-232 (ppm)	U-238 (ppm)	K (%)	De (Gy)[b]	DR (Gy/ka)	Age (ka)[b]
Unit A′	JMT2	17.3 ± 5.0	5.0 ± 1.4	1.5 ± 0.07	9.5 ± 1.0	3.6 ± 0.5	2.6 ± 0.5
Unit B	JMT4	12.3 ± 6.0	8.0 ± 1.0	1.7 ± 0.08	3.2 ± 0.3	4.1 ± 0.5	0.8 ± 0.1
Unit B	JMT5	11.6 ± 5.0	7.0 ± 1.4	1.8 ± 0.09	1.5 ± 0.5	3.9 ± 0.1	0.4 ± 0.1
Unit C	JMT6	8.9 ± 1.8	2.1 ± 0.5	1.96 ± 0.03	1 ± 0.07	2.9 ± 0.02	0.3 ± 0.04

[a] Refer trench section Fig. 7b for sample location.
[b] Equivalent dose (De) computed using minimum plus two sigma, water content assumed to be 10%, cosmic ray dose 150 micro-gray per year. Dating was carried out at Physical Research Laboratory, Ahmedabad. India.

refer to 1950 base line and hence in comparing OSL and radiocarbon ages, ~50a should be added to radiocarbon ages. For OSL dating, standard Single Aliquot Regeneration protocol on pure IRSL tested quartz was of Wintle and Murray (2006). The dispersion paleodoses were small and a mean age was selected. The radioactivity of samples were measured using the ZnS (Ag) thick source alpha counting technique and NaI(Tl) gamma ray spectrometry. The dose rate was calculated using elemental concentration of U, Th and K, assuming radioactive equilibrium and 10% water content. Cosmic ray contribution for the site was computed following Prescott and Stephen (1982).

The AMS radiocarbon measurements were carried out at Labor für Altersbestimmung und Isotopenforschung Christian-Albrechts-Universität, Kiel on charcoal samples. The sediment sample (Fig. 7b; Tables 2 and 3) from unit A′ (JMT2) sand lens within unit A provided OSL age of 2600 ± 500 yr. Radiocarbon age of detrital charcoal (H5) from unit B collected from the hanging wall in the overthrusted block yielded an age of 550 ± 50 yr BP and the sample from the same unit (JMT4) gave OSL age of 800 ± 100 yr. The sediment sample (JMT5) from unit B on the footwall yielded an OSL age of 400 ± 100 yr. The unit C capping the units A and B gave an OSL age of 300 ± 40 yr (JMT6), and the detrital charcoal (H2a) from the uppermost unit D gave an age of 225 ± 50 yr BP. Conjunctive use of two methods added an advantage towards validation of radiocarbon ages, besides the depositional and soil formation ages.

Stratigraphically, Event I along the F1 could be bracketed by the ages of unit A–A′ and unit B, i.e. between 2600 yr and 800 yr BP (Fig. 7b). Event II along F2 strand post-dated unit B (400 yr BP) and pre-dated unit C (300 yr BP) (Figs. 7b and 8). Unit A was displaced along F1 (Event I) and along F2 (Event II).

6. Discussion and conclusion

Any displacement along normal or reverse faulting or on elastic crack will propagate laterally as well as vertically with a reduction towards the tips of the faults along the strike (e.g., Gudmundsson, 1987a,b, 2000; Cartwright et al., 1995; Walsh et al., 2002; Davis et al., 2005). It has been suggested that as displacement occurs during major earthquake – fault grows, propagates laterally by acquiring more length along the strike (Walsh et al., 2002; Champel et al., 2002; Davis et al., 2005). Such phenomenon of lateral propagation of fault and related fold growth usually results in fluvial diversion, most commonly noticed in the active thrust-and-fold belts (Delcaillau et al., 1998; Champel et al., 2002; Bés de Berc et al., 2005; Malik and Mohanty, 2007; Simoes et al., 2007). The present study revealed occurrence of two parallel striking (NNW–SSE) fault scarps (HF1 and HF2) along the northwestern end of the Janauri anticline, which marks the frontal foreland fold extending for about 100 km (Figs. 2–4). The reduction in the height of the scarps towards NNW, i.e. from about 10 to 12 m near the hill range at Bamonwal-Siprian villages, reducing up to 8 m and as low as 2 m along HF1; and also from 6 to 8 m near the hill range, reducing up to about 1.5 m towards NNW along HF2 is suggestive of lateral propagation of fault and related folding in the frontal part of Himalaya (Figs. 2–4). This is further well justified by the deflection–diversion of Beas River channel in its present location (Figs. 3 and 4). The parallel striking HF1 and HF2 faults represents the propagation of deformation from two fault-related-fold segments – JF1 and JF2 respectively and represents the imbricated faults from the main Himalayan Frontal Thrust (HFT) system (Figs. 3a and 4).

The highly diffused and degraded morphology of HF1 scarp as compared to the HF2 suggests that the HF2 has experienced younger displacement during recent geological past. The length of the HF2 fault with 10 km and HF1 with 8 km also indicates that the HF2 is still accommodating recent movements and is comparatively more active than HF1.

The GPR helped us in identifying two northeast dipping low-angle thrust faults strands F1 and F2 (Fig. 5a and b). Exposed section in trench revealed only F2 strand with variable dip of ~32° in deeper part of the trench in northeast and graded to ~8° to almost horizontal in the southwest near surface displacing older gravel unit A and the overlying massive sand unit B. Flattening of fault in compression regime has been usually observed in thrust-fold-belt, e.g. in Algeria along El-Asnam fault (Meghraoui et al., 1988), in Himalaya along Chandigarh Fault (Malik et al., 2008) and along Tanda Fault in Pakistan (Kondo et al., 2005).

Total station profile gave scarp height of 6 m, whereas taking into consideration the top of the unit A exposed at the base of the trench and on the top of the scarp on hanging wall side gave a total vertical separation of about 8 m (Fig. 7c). The displacement of about 9 m (along F2 and c) during single event, and average fault angle of 25° measured from trench gave vertical separation of about 3.8 m and horizontal shortening of about 8.2 m during one single event. Therefore, the total vertical displacement of gravel unit A of about 8 m (Fig. 7c) suggests that this height has been acquired from at least two events, where the unit A got displaced along F1 strand during penultimate event and again along F2 strand during the latest event.

Radiocarbon and OSL ages shows that the earthquakes occurred during past ~2.6 ka (Fig. 7b; Tables 2 and 3). The OSL age of the finer layer in gravel unit (unit A) with 2600 yr gave the depositional age of the sediments (Fig. 7b and Table 3: sample no. JMT2). Therefore, the upper part of the gravel unit must be comparatively younger than 2600 yr. The OSL ages from unit B ranging from 800 yr up to 400 yr (Fig. 7b and Table 3: sample nos. JTM4 and JMT5) suggest that the deposition of the unit continued for longer span of time under the overbank depositional environment. The radiocarbon age of 550 yr BP and OSL age of 800 yr of unit B (Fig. 7b and Tables 2 and 3: sample nos. H5 and JMT4) from the overthrusted portion is suggestive of reworked charcoal fragment and sediments from deeper part. The unit C with OSL age of 300 yr caps the faulted succession (i.e. units A and B), and topmost unit D gave an age of 226 yr BP (Fig. 7b and Tables 2 and 3: samples JMT6 and H2a). It is inferred that the penultimate event (Event I) occurred along F1 strand displacing the unit A′–A, later covered by unit B

(Fig. 8a and b, Stages I and II), between 800 and 2600 yr. The latest event (Event II) occurred after the deposition of unit B and before the deposition of unit C, between 300 and 400 yr (Fig. 8c and d; Stages III and IV). The OSL and radiocarbon ages suggest that the event might have occurred somewhere around 1500–1600 AD and well before 1700 AD. The age of the penultimate event on the Hajipur fault is weakly constrained based on the wide range of the OSL ages between 800 yr (unit B) and 2600 yr (unit A′–A). Therefore, pin-pointing age of the event is difficult, but if we assume that the penultimate event occurred around 800 yr and taking into account the age of the latest event, it could be suggested a recurrence interval of about 500 yr.

Data from the trench and topographic profiles were used to estimate the geological slip rate and to work out the recurrence interval. The net displacement of about 9 m during the latest event, average angle of the fault ($\theta = 25^\circ$), vertical separation of the oldest unit A of about 7.5–8 m (Fig. 7c) and age of 2600 ± 500 yr from unit A–A′ were used. This gave the slip rate $= 7.6 \pm 1.7$ mm/yr, uplift rate $= 3.2 \pm 0.6$ mm/yr, shortening rate $= 6.9 \pm 1.4$ mm/yr and recurrence interval $= 1160 \pm 250$ yr. Considering the recurrence of 1100 yr obtained from the trench data and the occurrence of latest event it is suggested that the penultimate event probably occurred at around 1400–1500 yr BP. Paleoseismic investigations along the HFT in Central Himalaya suggest that ~1330–3250 years or more are needed to produce ~11–20 m slip during a single event and with time averaged slip of ~6–18 mm/yr (Kumar et al., 2006). Similarly, along the frontal part in eastern Nepal Lavé et al. (2005) suggest a single rupture event with slip of $17 + 6/-4$ m, and infer a return period ranging between 1800 and 3000 years. A rupture with >4–8 m of slip along 240 km long fault is associated to an earthquake with Mw 8.4 to Mw 8.8 Lavé et al. (2005). We concluded that the recurrence of large-magnitude events (M >7.5) along the Himalayan Frontal Thrust requires return time of about ~1000–1100 yr.

There is no report of historic event during the time frame of penultimate as well as latest event in the region. However, there is a report of event little north during 1555 AD – Kashmir event which caused ground fissures and rupture extend up to 100 km (Ambraseys and Jackson, 2003). Also it has been suggested that most recent event along Hajipur fault occurred during 1500 AD (?) (Malik et al., in press). Paleoseismic study along the HFT near Chandigarh city located about 150 km southeast of the trench site suggests latest event around 1400–1500 AD (Malik et al., 2008). This event has been identified along the southeastern end of the Chandigarh anticline (Fig. 1a). Given the uncertainties in dates, considering the historic and paleoseismic data it could be inferred that the latest event recorded in our trench could be the same occurred near Chandigarh at around 1400 AD or we are looking another major event during 1500–1600 AD.

GPS based convergence rate of 21 ± 3 mm/yr across the Nepal Himalaya (Bilham et al., 2001) is consistent with the slip rates obtained from folded fluvial terraces (Lavé and Avouac, 2000). Similarly the rate of 14 ± 1 mm/yr obtained from GPS between the sub-Himalaya and the Higher Himalaya across the Kangra reentrant during the period from 1995 to 2000 (Banerjee and Bürgmann, 2002) is consistent with convergence rate of 14 ± 2 mm/yr derived from balanced cross-sections (Powers et al., 1998). Paleoseismic investigations in the frontal part between Chandigarh and west of Nepal suggest fault slip rate of ~6–18 mm/yr (Kumar et al., 2006) and along HFT (Chandigarh fault) about 6.3 ± 2 mm/yr (Malik and Nakata, 2003). Present study gave slip rate along the Hajipur fault (HFT) is about 7.6 ± 1.7 mm/yr. This data enables a plausible suggestion that from the 14 ± 1 mm/yr, more than half is accommodated along the HFT making the frontal fault system the most active fault as compared to other hinterland faults.

This inference is significant for seismic hazard assessment because, presently, no sufficient paleoseismic data in this region of Himalayan foothills is available, this information will play important role in evaluating seismic hazard in this area along the thickly populated Indo-Gangetic Plain.

Acknowledgments

Financial support provided to JNM by DST, New Delhi (vide project No. DST/23(411)/SU/2003, now Ministry of Earth Sciences) is duly acknowledged. We are thankful to M.Tech and B.Tech students of IITK for their help in field. We are grateful to Prof. Gudmundsson for providing valuable comments and suggestions which helped in bringing more clarity to our paper. We are also thankful to Prof. Joao Hipprett for his suggestions and comments which added in improving our manuscript. We are also thankful to Prof. M. Meghraoui, IPG Strausbourg, France for valuable suggestions.

References

Ambraseys, N., Jackson, D., 2003. A note on early earthquakes in northern India and southern Tibet. Current Science 84 (4), 570–582.
Ambraseys, N., Bilham, R., 2000. A note on the Kangra Ms = 7.8 earthquake of 4 April 1905. Current Science 79 (1), 45–50.
Ambraseys, N.N., Douglas, J., 2004. Magnitude calibration of north Indian earthquakes. Geophysical Journal International 158, 1–42.
Avouac, J.P., Tapponnier, P., 1993. Kinematic model of active deformation in central Asia. Geophysical Research Letters 20, 895–898.
Banerjee, P., Bürgmann, R., 2002. Convergence across the northwest Himalaya from GPS measurements. Geophysical Research Letters 29 (13), 30-1–30-4. doi:10.1029/2002GL015184.
Bés de Berc, S., Soula, J.C., Baby, P., Souris, M., Christophoul, F., Rosero, J., 2005. Geomorphic evidence of active deformation and uplift in a modern continental wedge-top-foredeep transition: example of the eastern Ecuadorian Andes. Tectonophysics 399, 315–350.
Bilham, R., Gaur, V.K., 2000. Geodetic contributions to the study of seismotectonics in India. Current Science 79 (9), 1259–1269.
Bilham, R., Gaur, V.K., Molnar, P., 2001. Himalayan seismic hazard. Science 293, 1442–1444.
Bilham, R., 2001. Slow tilt reversal of the Lesser Himalaya between 1862 and 1992 at 78° E, and bounds to the southeast rupture of the 1905 Kangra earthquake. Geophysical Journal International 144, 713–728.
Bilham, R., Ambraseys, N., 2005. Apparent Himalayan slip deficit from the summation of seismic moments for Himalayan earthquakes, 1500–2000. Current Science 88 (10), 1658–1663.
Brown, L.D., Zhao, W., Nelson, K.D., Hauck, M., Alsdorf, D., Ross, A., Cogan, M., Clark, M., Liu, X., Che, J., 1996. Bright spots, structure and magmatism in southern Tibet from INDEPTH seismic reflection profiling. Science 274, 1688–1690.
Burbank, D.W., Verges, J., Munoz, J.A., Bentham, P., 1992. Coeval hindward- and forward-imbricating thrusting in the south-central Pyrenees, Spain: timing and rates of shortening and deposition. Geological Society of America Bulletin 104, 3–17.
Cartwright, J.A., Trudgill, B.D., Mansfield, C.S., 1995. Fault growth by segment linkage: an explanation for scatter in maximum displacement and trace length data from the Canyonlands Grabens of SE Utah. Journal of Structural Geology 17, 1319–1326.
Champel, B., Van der, B.P., Mugnier, J.L., Leturmy, P., 2002. Growth and lateral propagation of fault-related folds in the Siwaliks of western Nepal: rates, mechanisms, and geomorphic signature. Journal of Geophysical Research 107 (2111), 2-1–2-18.
Davis, K., Burbank, D.W., Fisher, D., Wallace, S., Nobes, D., 2005. Thrust-fault growth and segment linkage in the active Ostler fault zone, New Zealand. Journal of Structural Geology 27 (2005), 1528–1546.
Delcaillau, B., Deffontaines, B., Floissac, L., Angelier, J., Deramond, J., Souquet, P., Chu, H.T., Lee, J.F., 1998. Morphotectonic evidence from lateral propagation of active frontal fold; Pakuashan anticline, foothills of Taiwan. Geomorphology 24, 263–290.
DeMets, C., Gordon, R.G., Argus, D.F., Stein, D., 1994. Effect of recent revisions to the geomagnetic reversal time scale and estimates of current plate motions. Geophysical Research Letters 21, 2191–2194.
England, P.C., Molnar, P., 1997. The field of crustal velocity in Asia calculated from Quaternary rates of slip on faults. Geophysics Journal International 130, 551–582.
Gansser, A., 1964. The Geology of the Himalaya. Wiley Interscience, New York, pp. 189.
Gross, R., Green, A., Holliger, K., Horstmeyer, H., Baldwin, J., 2002. Shallow geometry and displacement on the San Andreas Fault near Point Arena based on

trenching and 3-D georadar surveying. Geophysical Research Letters 29 (20), 34-1–34-4.
Gudmundsson, A., 1987a. Geometry, formation and development of tectonic fractures on the Reykjanes Peninsula, southwest Iceland. Tectonophysics 139, 295–308.
Gudmundsson, A., 1987b. Tectonics of the Thingvellir fissure swarm, SW Iceland. Journal of Structural Geology 9, 61–69.
Gudmundsson, A., 2000. Fracture dimensions, displacements and fluid transport. Journal of Structural Geology 22, 1221–1231.
Hodges, K.V., 2000. Tectonics of the Himalaya and southern Tibet from two perspectives. Geological Society of America Bulletin 112, 324–350.
Hodges, K.V., Wobus, C., Ruhl, K., Schildgen, T., Whipple, K., 2004. Quaternary deformation, river steepening, and heavy precipitation at the front of the Higher Himalayan ranges. Earth and Planetary Science Letters 220, 379–389.
Iyengar, R.N., Sharma, D., 1999. Some earthquakes of the Himalayan region from historical sources. Journal of Himalayan Geology 20 (1), 81–85.
Kaneda, H., Nakata, T., Tsutsumi, H., Kondo, H., Sugito, N., Awata, Y., Akhtar, S.S., Majid, A., Khattak, W., Awan, A.A., Yeats, R.S., Hussain, A., Ashraf, M., Wesnousky, S.G., Kausar, A.B., 2008. Surface rupture of the 2005 Kashmir, Pakistan, earthquake and its active tectonic implications. Bulletin of the Seismological Society of America 98 (2), 521–557. doi:10.1785/0120070073.
Kumar, S., Wesnousky, W.G., Rockwell, T.K., Ragona, D., Thakur, V.C., Seitz, G.G., 2001. Earthquake recurrence and rupture dynamics of Himalayan Frontal Thrust, India. Science 294, 2328–2331.
Kumar, S., Wesnousky, S.G., Rockwell, T.K., Briggs, R.W., Thakur, V.C., Jayangondaperumal, R., 2006. Paleoseismic evidence of great surface rupture earthquakes along the Indian Himalaya. Journal of Geophysical Research 111, B03304. doi:10.1029/2004JB003309.
Kondo, H., Nakata, T., Akhtar, S.S., Wesnousky, S.G., Sugito, N., Kaneda, H., Tsutsumi, H., Khan, A.H., Khattak, W., Kausar, A.B., 2008. Long recurrence interval of faulting beyond the 2005 Kashmir earthquake around the northwestern margin of the Indo-Asian collision zone. Geology 36 (9), 731–734. doi:10.1130/G25028A.1.
Lyon-Caen, H., Molnar, P., 1983. Constraints on the structure of the Himalaya from the analysis of gravity anomalies and a flexural model of the lithosphere. Journal of Geophysical Research 88, 8171–8191.
Lavé, J., Avouac, J.P., 2000. Active folding of fluvial terraces across the Siwaliks Hills, Himalayas of central Nepal. Journal of Geophysical Research 105 (B3), 5735–5770.
Lavé, J., Yule, D., Sapkota, S., Basant, K., Madden, C., Attal, M., Pandey, R., 2005. Evidence for a Great Medieval Earthquake (1100 A.D.) in the Central Himalayas, Nepal. Science 307, 1302–1305.
LeFort, P., 1975. Himalayas, the collided range: present knowledge of the continental arc. American Journal of Science 275-A, 1–44.
Malik, J.N., Nakata, T., 2003. Active faults and related Late Quaternary deformation along the northwestern Himalayan Frontal Zone, India. Annals of Geophysics 46 (5), 917–936.
Malik, J.N., Nakata, T., Philip, G., Virdi, N.S., 2003. Preliminary observations from a trench near Chandigarh, NW. Himalaya and their bearing on active faulting. Current Science 85, 25.
Malik, J.N., Mohanty, C., 2007. Active tectonic influence on the evolution of drainage and landscape: geomorphic signatures from frontal and hinterland areas along Northwestern Himalaya, India. Journal of Asian Earth Sciences 29 (5–6), 604–618.
Malik, J.N., Sahoo, A.K., Shah, A.A., Rawat, A., Chaturvedi, A., 2007. Farthest recorded liquefaction around Jammu caused by October 8, 2005 Muzaffarabad earthquake of Mw 7.6. Journal of the Geological Society of India 69, 39–41.
Malik, J.N., Nakata, T., Philip, G., Suresh, N., Virdi, N.S., 2008. Active fault and paleoseismic investigation: evidence of historic earthquake along Chandigarh Fault in the frontal Himalayan zone, NW India. Journal of Himalayan Geology 29 (2), 109–117.
Malik, J.N., Shah, A.A., Sahoo, A.K., Puhan, B., Banerjee, C., Shinde, D.P., Juyal, N., Singhvi, A.K., Rath, S.K. Active fault, fault growth and segment linkage along the Janauri anticline (frontal foreland fold), NW Himalaya, India. Tectonophysics, in press.
McCalpin, J., 1996. Paleoseismology. Academic Press, 588 pp.
Meghraoui, M., Jaegy, R., Lammali, K., Albarede, F., 1988. Late Holocene earthquake sequences on the El Asnam (Algeria) thrust fault. Earth and Planetary Science Letters 90, 187–203.
Nakata, T., 1972. Geomorphic History and Crustal Movements of Foothills of the Himalaya. Inst. of Geography, Tohuku Univ., Sendai, pp. 77.
Nakata, T., 1989. Active faults of the Himalaya of India and Nepal. Geological Society of America Bulletin, Special Paper 232, 243–264.
Nakata, T., Otsuki, K., Khan, S.H., 1990. Active faults, stress field, and plate motion along the Indo-Eurasian plate boundary. Tectonophysics 181, 83–95.
Nakata, T., Tsutsumi, H., Khan, S.H., Lawrence, R.D., 1991. Active faults of Pakistan: map sheets and inventories, Special publication 21, Research Center for Regional Geography. Hiroshima University, Hiroshima.
Ni, J., Barazangi, M., 1984. Seismotectonics of the Himalayan collision zone: Geometry of the underthrusting Indian plate beneath the Himalaya. Journal of Geophysical Research 89, 1147–1163.
Oatney, E.M., Virdi, N.S., Yeats, R.S., 2001. Contribution of Trans-Yamuna active fault system towards hanging wall strain release above the décollement, Himalayan foothills of Northwest India. Journal of Himalayan Geology 22 (2), 9–27.
Prescott, J.R., Stephen, L.G., 1982. The contribution of cosmic radiation to the environmental dose for thermoluminescence dating. PACT 6, 17–25.
Powell, C.McA., Conaghan, P.J., 1973. Plate tectonics and the Himalayas. Earth and Planetary Science Letters 20, 1–12.
Powers, P.M., Lillie, R.J., Yeats, R.S., 1998. Structure and shortening of the Kangra and Dehra Dun reentrants, Sub-Himalaya, India. Geological Society of America Bulletin 110, 1010–1027.
Raiverman, V., Srivastava, A.K., Prasad, D.N., 1994. Structural style in Northwestern Himalayan Foothills. Himalayan Geology 15, 263–282.
Seeber, L., Armbruster, J.G., Quittmeyer, R.C., 1981. Seismicity and continental subduction in the Himalayan arc. In: AGU, Geodynamics Ser., 5. Washington, D.C.
Seeber, L., Armbruster, J.G., 1981. Great detachment earthquakes along the Himalayan arc and long-term forecasting. In: Simpson, D.W., Richards, P.G. (Eds.), Earthquake Prediction – an International Review, 4. AGU, pp. 259–279.
Seeber, L., Gornitz, V., 1983. River profiles along the Himalayan arc as indicators of active tectonics. Tectonophysics 92, 335–367.
Simoes, M., Avouac, J.P., Chen, Y.G., Singhvi, A.K., Wang, C.Y., Jaiswal, M., Chan, Y.C., Bernard, S., 2007. Kinematic analysis of the Pakuashan fault tip fold, west central Taiwan: shortening rate and age of folding inception. Journal of Geophysical Research 112, B03S14. doi:10.1029/2005JB004198.
Stöcklin, J., 1980. Geology of Nepal and its regional frame. Journal of the Geological Society (London) 137, 1–34.
Stuiver, M., Polach, H.A., 1977. Discussion: reporting of ^{14}C data. Radiocarbon 19 (3), 355–363.
Stuiver, M., Reimer, P.J., Bard, E., Beck, J.W., Burr, G.S., Hughen, K.A., Kromer, B., McCormac, G., Van der Plicht, J., Spurk, M., 1998. INTCAL98 radiocarbon age calibration, 24,000-0 cal BP. Radiocarbon 40, 1041–1083.
Tapponnier, P., Ryersonb, F.J., Van der Woerd, J., Mériaux, A.S., Cécile, L., 2001. Long-term slip rates and characteristic slip: keys to active fault behaviour and earthquake hazard. Comptes Rendus de l'Academie des Sciences: Earth and Planetary Science 333, 483–494.
Valdiya, K.S., 1980. The two intracrustal boundary thrusts of the Himalaya. Tectonophysics 66, 323–348.
Valdiya, K.S., 1992. The main boundary thrust zone of Himalaya, India. Annales Tectonicae 6, 54–84.
Validya, K.S., 2003. Reactivation of Himalayan frontal fault: implications. Current Science 85 (7), 1013–1040.
Wallace, K., Bilham, R., Blume, F., Gaur, V.K., Gahalaut, V., 2005. Surface deformation in the region of the 1905 Kangra Mw = 7.8 earthquake in the period 1846–2001. Geophysical Research Letters 32 (15), L15307. doi:10.1029/2005GL022906.
Walsh, J.J., Nicol, A., Childs, C., 2002. An alternative model for the growth of faults. Journal of Structural Geology 24, 1669–1675.
Wesnousky, S.G., Kumar, S., Mohindra, R., Thakur, V.C., 1999. Uplift and convergence along the Himalayan Frontal Thrust. Tectonics 18 (6), 967–976.
Wintle, A.G., Murray, A.S., 2006. A review of quartz optically stimulated luminescence characteristics and their relevance in single-aliquot regeneration dating protocols. Radiation Measurements 41, 369–391.
Yeats, R.S., Nakata, T., Farah, A., Fort, M., Mirza, M.A., Pandey, M.R., Stein, R.S., 1992. The Himalayan frontal fault system. Annales Tectonicae 6 (Suppl.), 85–98.
Yeats, R.S., Sieh, K., Allen, C.R., 1997. Geology of Earthquakes. Oxford Univ. Press, 568 pp.
Yeats, R.S., Hussain, A., 2006. Surface Features of the Mw 7.6, 8 October 2005 Kashmir Earthquake, Northern Himalaya, Pakistan: Implications for the Himalayan Front. Abstract. Seismol. Soci. America.
Zhao, W., Nelson, K.D., Project INDEPTH Team, 1993. Deep seismic reflection evidence for continental underthrusting beneath southern Tibet. Nature 366, 557–559.